Bromine interaction with Si(100)-2×1: Chemisorption and initial stages of etching

D. Rioux, M. Chander, Y. Z. Li, and J. H. Weaver
Department of Materials Science and Chemical Engineering, University of Minnesota, Minneapolis, Minnesota 55455
(Received 1 November 1993)

The dissociative chemisorption of Br_2 on Si(100)-2×1 at 300 K and the initial stages of layer-by-layer etching at high temperature have been studied with scanning tunneling microscopy. The Si surface maintains the 2×1 reconstruction upon Br exposure with low-yield adsorption-induced etching at room temperature. Annealing Br-covered surfaces at temperatures up to ~800 K results in thermally activated etching, but the yield is low. Higher-yield etching of the steps and terraces takes place at ~900 K. Healing of this etched surface begins at ~1000 K, and there is complete Br desorption and restoration of the pre-etch morphology by ~1100 K. Etching under continuous bombardment by Br_2 at 900 K was studied by varying the halogen flux while keeping the fluence constant. Quantitative analyses of images obtained during the early stages of continuous etching showed differences in the morphologies that offered insight into etching mechanisms.

I. INTRODUCTION

Etching semiconductor surfaces with halogens has assumed growing importance in the dry processing of semiconductors, and it is important to gain a deeper understanding of the etch processes so that they can be better controlled.[1] Scanning tunneling microscopy (STM) can be used to investigate adsorption and etching phenomena with atomic resolution, yielding insight into surface structures and the kinetics of etching. For example, Boland and Villarrubia[2] examined Cl_2 interactions with Si(111)-7×7 and demonstrated that most of the adatom layer was stripped away to reveal the underlying Si rest-atom layer when a Cl-saturated surface was annealed. Patrin and co-workers[3,4] investigated Cl and Br etching of GaAs(110), and related the etch mechanisms and the resulting morphologies to the sample temperature, etchant flux, and step orientation. Recently, Chander and co-workers[5,6] discovered that a bounded steady-state morphology results from Br etching of Si(100)-2×1 at 900 K. This atomic-layer etch mode is characterized by a 3×1 surface structure, the formation of single-layer etch pits on the terraces, and preferential etching along dimer rows.

In this paper we report a STM investigation of bromine chemisorption on Si(100)-2×1 and the initial stages of layer-by-layer etching at elevated temperatures. We show that Br_2 dissociates at room temperature and doubly occupies the Si dimers, confirming the interaction between dangling bonds of the same dimer. We then examine desorption characteristics, etching, and regrowth as surfaces with Br-saturated dangling bonds are annealed at successively higher temperatures. Surface morphologies are discussed in terms of thermally activated desorption channels and diffusion of surface species, including vacancies. Finally, we consider step profiles at high temperature as a function of halogen flux at a fixed fluence (total exposure). Quantitative analyses of kink-kink separation, kink length, step roughness, and defect density yield insight into the formation of volatile etch products on terraces and at step edges.

II. EXPERIMENT

The experiments were performed in an ultrahigh-vacuum chamber equipped with a Park Scientific Instruments STM (base pressure 5×10^{-11} Torr). Silicon wafers oriented within 0.2°–0.05° of (100) and miscut toward [110] were rinsed in ethanol prior to introduction into the vacuum. The wafers were degassed at 600 °C for several hours and then flashed to 1200 ° for 1–2 min. This procedure has been shown to produce clean, well-ordered Si(100)–2×1.[7] Analysis of images of the clean surface indicated a defect density of $\sim1.3\times10^{13}$ cm^{-2}, primarily in the form of missing dimers. Sample temperatures were monitored with an optical pyrometer and were accurate to ±20 K. Electrochemically etched tungsten tips were cleaned using electron bombardment. Scan dimensions were calibrated using the Si(100)-2×1 lattice and the height of monatomic steps. All STM micrographs were acquired in a constant current mode at room temperature. Some show slight distortions because they were not corrected for thermal drift. Individual scan lines in the images were "tilt" corrected to remove low-frequency oscillations, and a (FFT) fast Fourier transform filter was used to remove a high-frequency oscillation in Fig. 2. The data were not further processed before their presentation here as grayscale images.

An electrochemical cell[8] consisting of a AgBr pellet doped with $CdBr_2$ was used as a Br_2 source. Under an applied voltage, halogen ions diffuse to a Pt mesh electrode where they desorb as Br_2. The sample was placed ~3 cm from the mesh during exposures, and then loaded onto the STM stage in a different part of the chamber. The chamber pressure remained below 1×10^{-10} Torr during dosing. Exposures were calibrated using Faraday's law. Stable cell currents in the range 5–80 μA yielded fluxes from $\sim1.6\times10^{13}$ to 2.5×10^{14} molecules

per second. The total exposures are quoted in terms of fluence in units of mA sec.

III. RESULTS AND DISCUSSION

A. Dissociative chemisorption

Figure 1(a) shows an 80×80-Å^2 area of a Si(100)-2×1 surface after exposure to a Br_2 fluence of 0.3 mA sec at room temperature. Comparison to clean surface images indicates that the bright rows are Si dimer rows oriented along $[0\bar{1}1]$, labeled Si. Bromine exposure leads to scattered adsorption sites that can be recognized by their darker appearance, labeled Br. Varying degrees of contrast between dark- and light-colored dimers were achieved by changing the bias voltage. The sharp contrast evident in Fig. 1(a) occurred for sample bias voltages near -1.0 V. No such high-contrast dimer features were observed on the clean Si surface near this bias. The black areas in the scan, such as in the lower left corner, represent surface defects. While most of these are missing dimer defects, labeled MD, others are related to residual water adsorption.[9] Figure 1(b) shows that exposure to 1.8 mA sec increased the density of the adsorption features such that relatively few Si dimers remained Br free. These Br-free dimers appears as bright objects in Fig. 1(b). Many of them are individually resolved while short segments remain undifferentiated, as in Fig. 1(a). From many experiments using different tips and samples we have found that, in general, clean Si dimers cannot be individually resolved following low Br exposure, in contrast to the clean surface. As the Br concentration increases to ~1 monolayer, however, clean dimers are again resolved, as in Fig. 1(b). Therefore, we attribute this effect to dangling-bond saturation at moderate coverages that reduces the localized nature of the surface electronic structure rather than to a tip-induced effect.

Inspection shows that there is an increase in the number of defects from $\sim1.3\times10^{13}$ cm^{-2} for the clean surface, to $\sim1.7\times10^{13}$ cm^{-2} after exposure to 0.3 mA sec [Fig. 1(a)], to $\sim4.1\times10^{13}$ cm^{-2} after 1.8 mA sec [Fig. 1(b)]. Though rare on clean Si(100), a significant number of missing-atom defects appeared after Br_2 exposure, labeled MA in Fig. 1(b). For the clean surface, these single-atom vacancies have short lifetimes and usually convert to dimer vacancies.[10] For Br-exposed surfaces, however, the single-atom vacancies were stable over long periods of time and repeated scans, as were all post-exposure features. The majority of the Si atoms accompanying missing-atom defects appear Br terminated. The increase in defect density and the creation of missing-atom defects can be attributed to a low-yield, adsorption-induced etch process that is active even at temperatures below 300 K. In support of this picture, we note that Jackman, Price, and Ford[11] found immediate desorption of Si-Br species, primarily $SiBr_4$ upon exposing Si(100) to Br_2 at low temperatures, a process that ceased when the halogen supply was interrupted. We attribute the changes in the surface defect density evident in Fig. 1 to spontaneous etching processes that are an immediate consequence of the adsorption and dissociation of the Br_2 molecules, as will be discussed below.

While Br adsorption at 300 K removes the occasional Si dimer or atom, it does not disrupt the underlying 2×1 surface mesh. To visualize the adsorption structure, we acquired dual bias images for the surface after a 3.0 mA sec exposure which resulted in Br termination of all dimer dangling bonds. Figure 2 shows a 2×1 reconstruction in both images and reveals that each dimer unit is

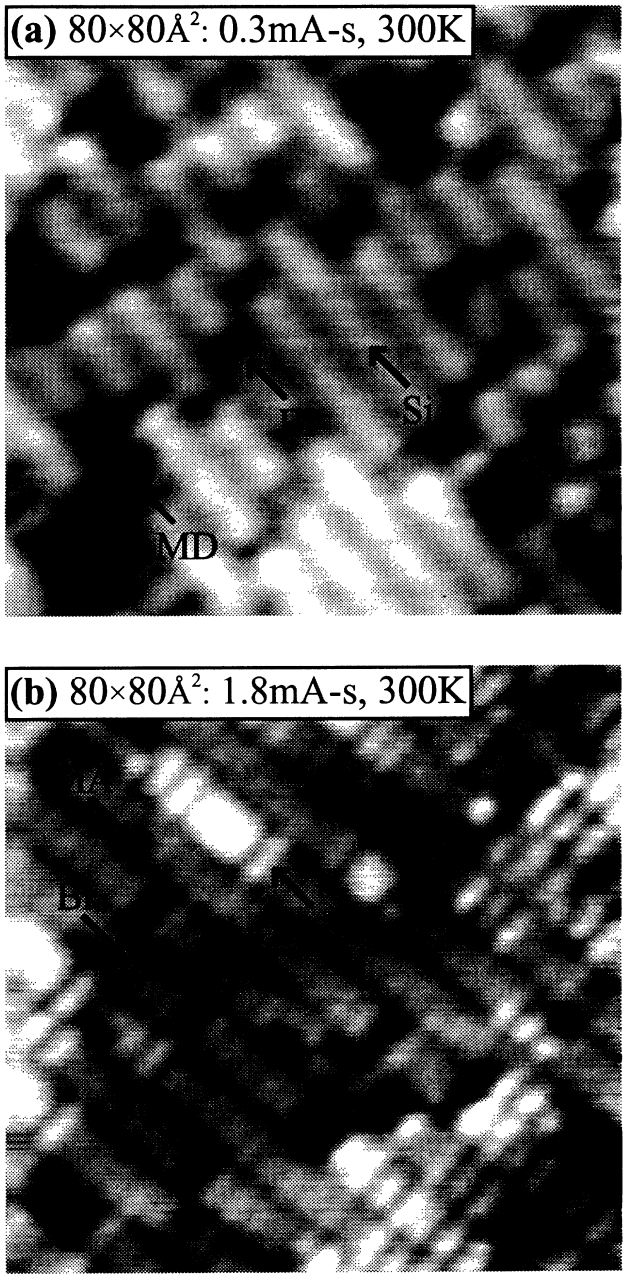

FIG. 1. Occupied-state images (-1.1 V, 0.2 nA) of Si(100)-2×1 exposed to Br_2 fluences of (a) 0.3 mA sec and (b) 1.8 mA sec at room temperature. The brightest features are clean Si dimers, labeled Si. Br adsorption sites (Br) are individually resolved and appear grey. Surface defects appear black, labeled MD for missing dimers and MA for missing atoms. Exposure to 1.8 mA sec produces a surface where the minority population corresponds to Si dimers that are Br free, as indicated by the bright features in (b).

composed of two bright features. This atomic resolvability at both positive and negative biases, which is observed at all bromine coverages, is in contrast to clean Si(100)-2×1, where the dimers appear as single protrusions in filled-state images and resolvable atomic features only in empty-state images.[12] This behavior allows a distinction to be made between Br-terminated and clean Si dimers in a given scan, much like varying the bias voltage as employed above for lower Br coverage.

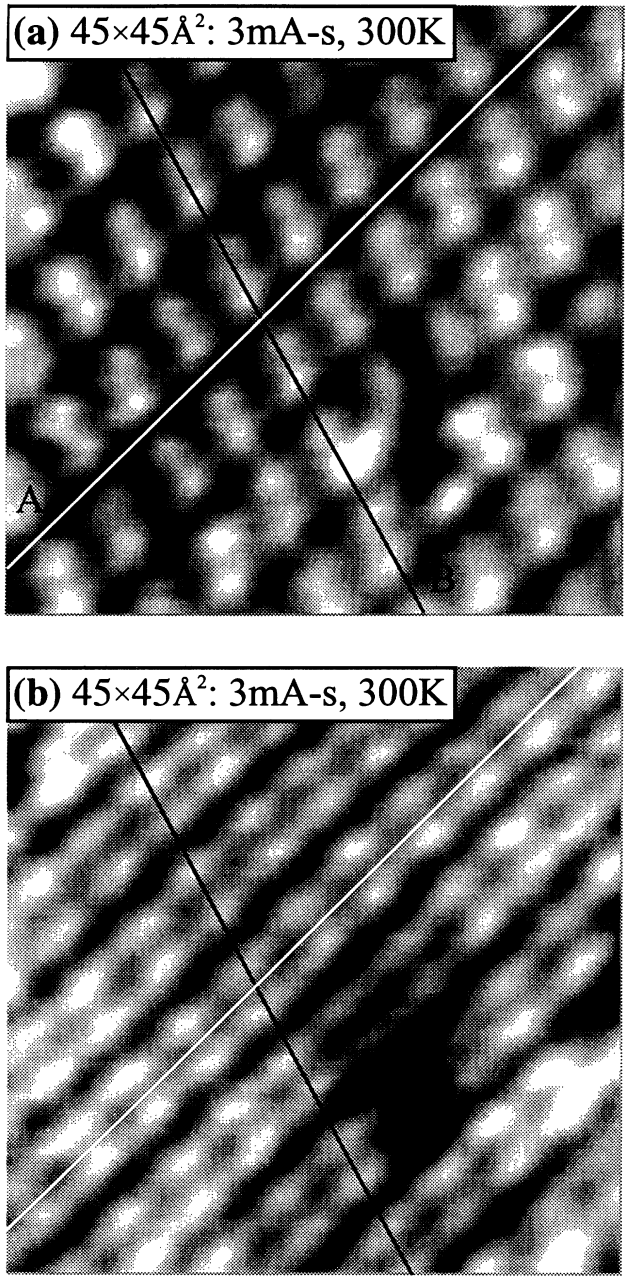

FIG. 2. Dual bias images (±0.9 V, 0.1 nA) of a Br-saturated Si(100)-2×1 surface after exposure to 3 mA sec. The bright features that appear in pairs are indicative of dissociative Br_2 chemisorption to dimer dangling bonds. Line *A* lies in the trough between dimers rows in both (a) and (b). Its position appears to be different, however, because the occupied and unoccupied states of the surface are not spatially coincident. Line *B* shows that the adsorption structure is parallel to the dimer-bond direction.

Figure 2 shows that there is a shift in the nodal features in the filled- and empty-state images. Line *A* passes between dimer rows in Fig. 2(a) but splits the paired features of the same row in Fig. 2(b). This is distinct from what is seen for clean Si(100)-2×1 (Ref. 12) and H-Si(100)-2×1[13,14] where occupied and unoccupied state dimer row features coincide spatially. The fact that the paired nodal features are symmetric with respect to the dimer unit in both images suggests an adsorption geometry that is symmetric about the Si dimer row direction. Line *B* passes through pairs of bright features perpendicular to the dimer row direction, suggesting an adsorption geometry oriented along the Si dimer bond direction. These results are consistent with *x*-ray standing-wave analysis[15] of the Br-saturated Si(100)-2×1 surface, confirming that Br_2 adsorption is dissociative at room temperature and that the surface consists of symmetric, Br-terminated Si dimers.

For room-temperature exposures, the Si dimers were either occupied by two Br adsorbate atoms or were left clean. Singly occupied dimers were not observed. On clean Si(100)-2×1, the dimer dangling bonds interact via a π bond[16] that can affect adsorption characteristics. In particular, if the π bonds are stronger than the repulsive interaction between adsorbate atoms, then double occupation of dimers is thermodynamically preferred. This has been verified for atomic hydrogen adsorption on Si(100)-2×1.[13,17,18] Because π bonding is intrinsic to the dimerized surface, preferential pairwise occupation of dimers has been predicted for adsorbates other than hydrogen,[13,17,18] and the adsorption characteristics described here fulfill this prediction.

B. Thermal desorption and surface etching

Si(100)-2×1 surfaces exposed to 3.0 mA sec, which saturates the dimer dangling bonds, served as the starting point for studies of bromine desorption and thermally activated etching. High-resolution images obtained after annealing at 700 K for 30 sec showed that most dimer dangling bonds remained Br terminated, but an increase in the defect density to $\sim 6.0\times10^{13}$ cm^{-2} demonstrated that thermally activated etching had started. These results suggest that more than one monolayer of Br was adsorbed on the surface after the exposure, and are consistent with temperature-programmed desorption (TPD) data that showed that Br may occupy, without apparent limit, chemisorption states that result in the desorption of $SiBr_3$ and $SiBr_4$ between 400 and 700 K.[11]

Figure 3(a) was obtained after annealing the Br-exposed surface to 800 K for 30 sec. Bright features indicative of Br-free Si dimers reappeared within previously homogeneous Br-terminated areas. This is expected since Br depletion due to desorption of Br-rich Si species and Br_2 leads to redistribution of the adsorbate. High-resolution scans revealed no singly occupied dimers, demonstrating that Br desorption and redistribution are both influenced by the π-bond interaction between dangling bonds. Analogous paired removal from doubly oc-

cupied dimers for the monohydride phase of H-Si(100) was also attributed to the influence of π-bonding.[13,17,18]

Annealing to 900 K for 30 sec produced a dramatic change in the surface morphology, as represented in Fig. 3(b). This surface consists of 2×1-reconstructed chains labeled (C) and two-dimensional islands (I) that are 1.4 Å in height, missing-atom and missing-dimer defects, and single-layer-deep etch pits (P). Small 3×1-reconstructed domains have also appeared, the formation of which is described in detail elsewhere.[6] High-resolution scans indicate that approximately half of the dimers in the chains, islands, pits, and terraces are still Br terminated. Many of the chains and islands represent regrowth structures that are similar to growth structures observed in Si homoepitaxy.[19–22] For etching, however, the Si atoms that constitute the islands were released by desorption events involving half of a dimer, leaving the other atoms free to diffuse. These atoms diffuse until they are incorporated at step edges trapped by existing islands, or form new islands. Etching and regrowth near S_B step edges make the step contours very ragged, as is evident in Fig. 3(b). The regrowth structures are anisotropic and identical to those observed under conditions of continuous Br exposure at 900 K.[5] Similar features have been observed after etching Si(100) with hydrogen and oxygen.[23,24]

Figure 3(c) shows that annealing a Br-saturated surface at 1000 K resulted in further etching and to much more regular step profiles compared to Fig. 3(b). The disappearance of regrowth islands and dimer chains reflects a combination of $SiBr_x$ desorption and Si incorporation at step edges. The healing of etch pits within terraces can be related to the diffusion of vacancies to step edges, where they are annihilated. Such vacancy diffusion has been observed at temperatures as low as 490 K for Si(100).[25,26]

Finally, annealing at 1100 K resulted in a regularly stepped, dimer-reconstructed Si(100)-2×1 surface with a defect density that approached the value for the clean surface. Images taken under different tunneling bias conditions demonstrated that no Br remained, in agreement with TPD data.[11]

C. Initial stages of continuous etching at 900 K

The previous two sections have emphasized adsorption-induced etching and thermally activated etching. Etching under conditions of continuous Br_2 exposure was also investigated as a function of flux at constant temperature and fluence. Under these conditions, molecular impingement and thermal activation occur simultaneously. The measurements were done after exposure at 900 K because detailed investigations at temperatures between 600 and 1100 K (Ref. 27) showed that surface modification was more significant at 900 K than at lower temperatures, and that the resulting surface remained more ordered than at higher temperatures. We found that a "standard" fluence of 0.8 mA sec allowed quantitative structural analyses of step-edge roughness. The fluence produced a surface morphology that had progressed approximately one third of the way to the steady-state etch conditions.[5]

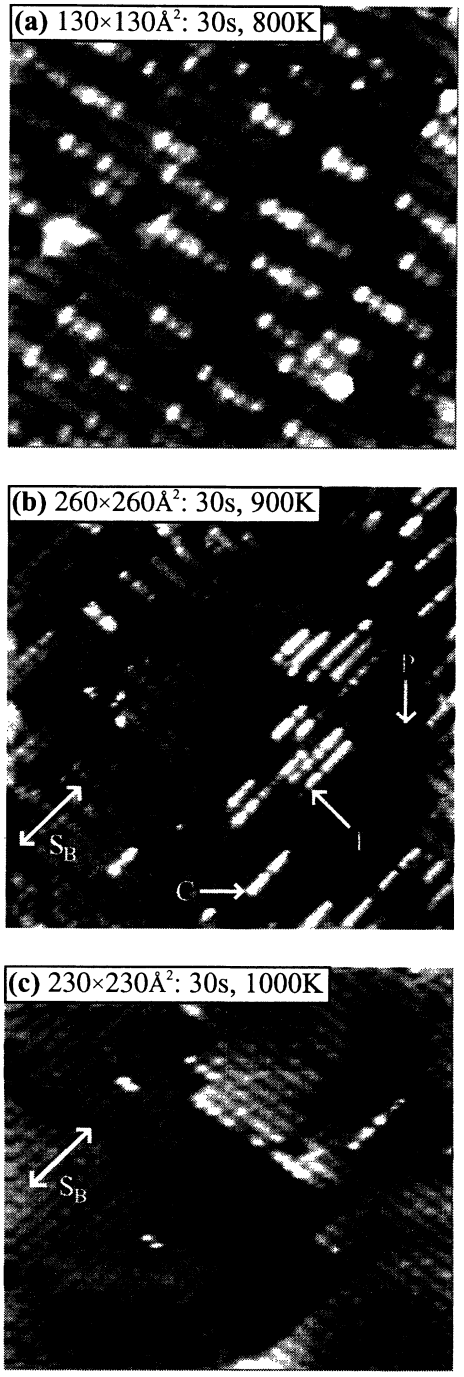

FIG. 3. Occupied-state images obtained after annealing a Br-covered surface for $800 \leq T \leq 1000$ K. (a) Bright features are clean Si dimers from which Br has been removed during processes that produce volatile etch products. (b) Terrace etching is apparent and the profile of the original S_B passing from lower left to upper right is poorly defined. Dimer chains (C) and 2×1 islands (I) have coalesced from material liberated during the etch. Single-layer etch pits (P) are apparent on the terraces. (c) The etch damage evident in (b) has largely been repaired by Si atom and vacancy diffusion, and most of the Br has desorbed.

Figures 4(a) and 4(b) show the effects of flux for a surface exposed to a 10-μA flux for 80 sec, corresponding to low flux (LF). Figures 4(c) and 4(d) show the equivalent results for exposure to an 80-μA flux for 10 sec, corresponding to high flux (HF). While the surface morphologies are distinct, both HF and LF etching yield Si regrowth islands, single-layer-deep etch pits, and significant step-edge modification relative to the clean surface. Inspection of a large number of such images for the "standard" fluence using fluxes between 5 and 80 μA revealed that islands and chains nulceated isotropically. There was no preference for nucleation at step edges over terraces, no "denuded zones" near S_B steps, and no preference for S_A steps over S_B steps. This differs from homoepitaxial growth of Si, which favors accommodation at S_B steps and the formation of denuded zones near S_B step edges.[28,29] Since denuded zones are formed as a consequence of anisotropic diffusion of Si, where diffusion is faster along the dimer row direction, their absence suggests that the diffusion characteristics on the Br-covered surface are different than the bare Si(100) surface. In addition, preferential etching at *B*-type steps may counteract the tendency to form denuded zones by liberating Si for local regrowth. There was no discernible dependence of regrowth island size on Br_2 flux, terrace type, or terrace size, except for very narrow terraces where the regrowth density was negligible.

Analysis shows that the shape anisotropy of the regrowth structures was independent of flux with characteristic values in the range 2–7 after etching at 900 K. These compare to values of 10–15 for Si homoepitaxy.[19–22] The differences reflect a combination of factors. First, regrowth structures are themselves subjected to etching that occurs preferentially along the dimer row direction. This leads to stunted growth structures. Second, shape anisotropies are temperature dependent,[22] and the high temperature used here can cause regrowth features to assume a lower shape anisotropy. Finally, island coarsening can occur during the sample quench to room temperature, an effect that could reduce the shape anisotropy somewhat.[22]

The differences in surface morphologies produced by high and low flux etching can be summarized as follows. First, the etch pit density on terraces is greater on HF surfaces than on LF surfaces, as is evident from Figs. 4(a) and 4(c). Second, the vacancy islands are generally smaller on HF surfaces. Nonetheless, vacancy area measurements on the terraces reveal that the etch fraction is greater for HF surfaces than for LF surfaces ($\sim$19% vs $\sim$13%). Thus the higher flux at fixed fluence produces smaller etch pits, but their density is larger and there is more terrace etching. However, the density of regrowth islands and their total area increases for HF surfaces, consistent with greater terrace and step-edge etching and

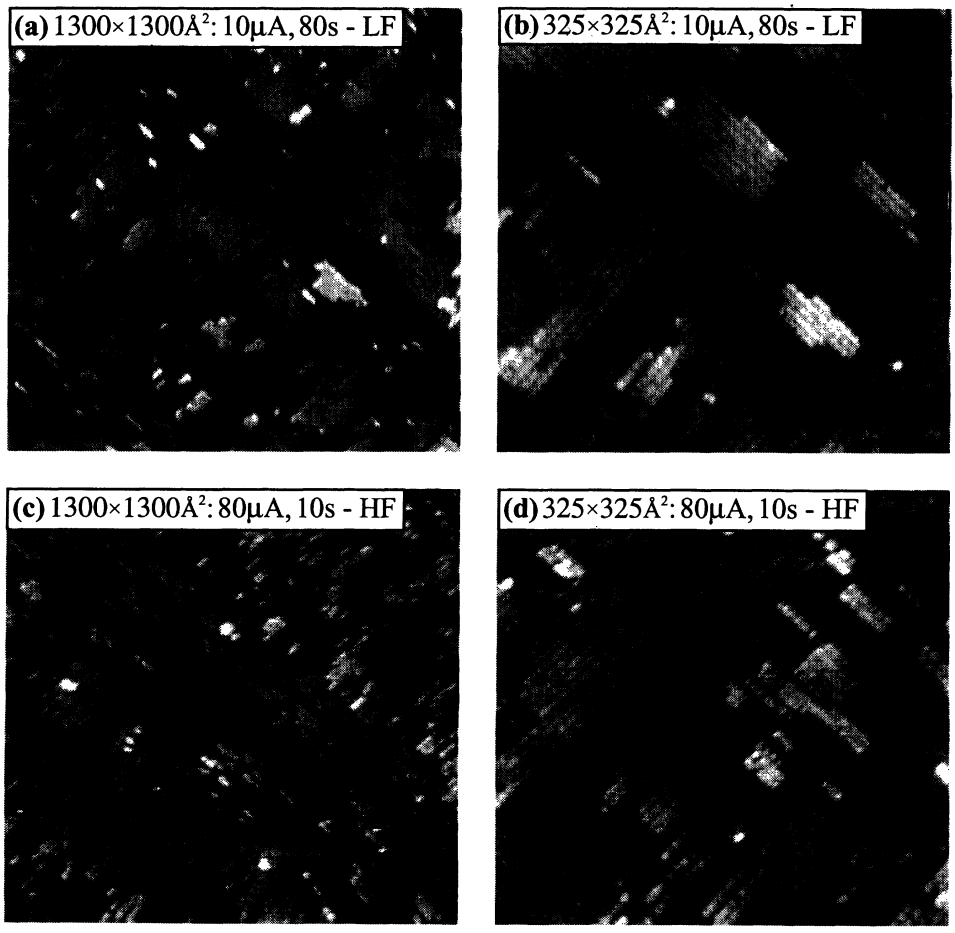

FIG. 4. Images taken after etching under conditions of LF [low flux, images (a) and (b)] and HF [high flux, images (c) and (d)] for times that produce the same fluence. The large-scale images show that the HF surfaces have rougher *B*-type step edges, a larger number of etch pits, and a greater amount of regrowth. The small-scale images show detailed differences in step-edge roughness and in regrowth structure morphology.

the release of more Si atoms for regrowth. Third, the linearity of the S_B step edges at moderate length scales is more severely degraded for HF surfaces, displaying more frequent etch fingers into the upper terrace, while the step profiles on LF surfaces retain longer straight segments. Finally, Figs. 4(b) and 4(d) show that regrowth structures have more missing dimers on HF surfaces and that island boundaries are less regular.

D. Flux dependence of S_A and S_B step profiles

Inspection of the S_B step edges of Fig. 4 shows that those on HF surfaces are more ragged on short length scales than those on LF surfaces. In contrast, the S_A step profiles for HF and LF surfaces show less apparent dependence on flux. Quantitative analysis of the dependence of step-edge roughness on flux can be done via the deviation-deviation correlation function $G(r) = \langle [h_0 - h(r)]^2 \rangle$.[30] Here r is the range parallel to a step edge and $h(r)$ is the in-plane deviation from the origin h_0 that defines a straight step edge, as depicted in the inset of Fig. 5. Both r and $h(r)$ are integers, so that distances are measured in dimer row units.

Figure 5 shows $G(r)$ for ranges $1 \leq r \leq 20$ parallel to S_A and S_B step edges on surfaces exposed to 0.8 mA sec for fluxes of 5–80 μA. Clean surface curves are included for comparison. For A-type step edges, $G(r)$ demonstrates that the step roughness increases manyfold upon Br exposure, Fig. 5(a), even at low flux. The roughness variations generally increase with flux, but the roughness does not scale simply. The relatively small variation in $G(r)$ between HF and LF surfaces indicates that improved statistics may impose more order on the plot. Significantly, the difference in $G(r)$ between HF and LF surfaces is not large. This quantifies the observation above that S_A steps had similar appearances for HF and LF exposures. For S_B steps, the $G(r)$ values are plotted on a logarithmic scale, Fig. 5(b), because $G(r)$ extends over a greater range of values. The observation that S_B steps are rougher for HF than LF surfaces manifests itself as a large change in the magnitude of $G(r)$ with increasing flux. Unlike S_A steps, the roughness of S_B increases monotonically with flux at all r values. The trend to greater deviations for both S_A and S_B steps with increasing flux establishes that the etchant arrival rate, and hence the local concentration of Br on the surface affects the step-edge profiles. Thus higher concentrations promote etching and produce rougher steps.

The resistance of S_A steps to roughening due to preferential removal along the dimer row direction (parallel to the step edge) is partially overcome by increasing the flux. Although the S_B steps are also made rougher by this treatment, on average the S_A steps are roughened more than S_B steps relative to the clean surface. The ratio of $G(r)$ between the etched and clean surfaces for moderate length scales ($r \sim 20$) on both HF and LF surfaces demonstrates this. For S_A steps, this ratio for $r = 20$ ranges from 7.0 for LF surfaces to 10.5 HF surfaces, while for S_B steps the range is 4.0 to 7.5. Hence, although S_B steps are etched preferentially due to a larger number of kink sites and the etch anisotropy along the dimer row direction, the S_A steps are also significantly attacked. Indeed, both step profiles are ill-defined in more advanced stages of continuous etching at 900 K.[5]

Analyses of the separation of kinks along a given step edge and of the length of kinks perpendicular to the step edge also reflect the influence of the flux. Again, kink separations and kink lengths are measured in dimer row units, denoted by the integers n and l, as defined in the inset of Fig. 6. The average values of n and l are plotted as a function of flux with clean surface values (zero cell current) plotted for comparison. From Fig. 6(a), the

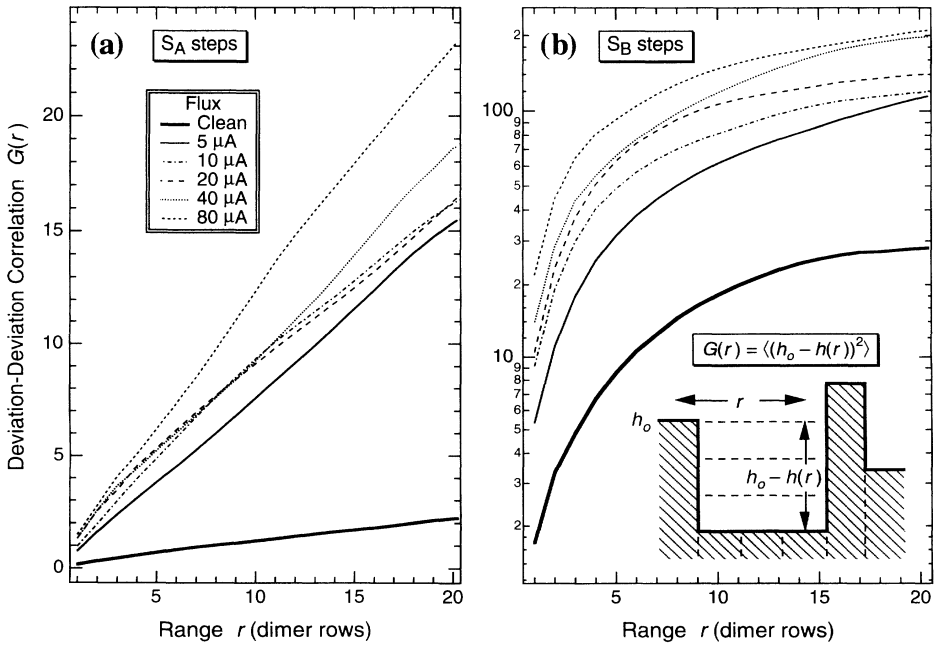

FIG. 5. Deviation-deviation correlation formations for (a) S_A step edges and (b) S_B step edges on surfaces exposed at 900 K to 0.8 mA sec Br_2 using a range of flux, characterized by the cell currents. Clean surface results are shown for comparison. The inset in (b) defines the range r parallel to a step edge and the deviation $h_0 - h(r)$ perpendicular to the step edge in units of dimer rows. The curves demonstrate that both steps are roughened with increasing flux.

average kink separation decreases with increasing flux for both types of steps at 900 K for the standard fluence. This is consistent with the step-edge roughness calculated above: Since $G(r)$ increases with flux at small r, the distance between kinks must decrease. Figure 6(b) shows that the average kink length increases after etching the clean surface. This demonstrates that Si removal from steps is not uniform, and that steps do not retreat by "step flow." Were step flow the case, there would also be little change in $G(r)$ with Br exposure. Finally, Fig. 6(b) shows that the average kink length depends only weakly on the flux.

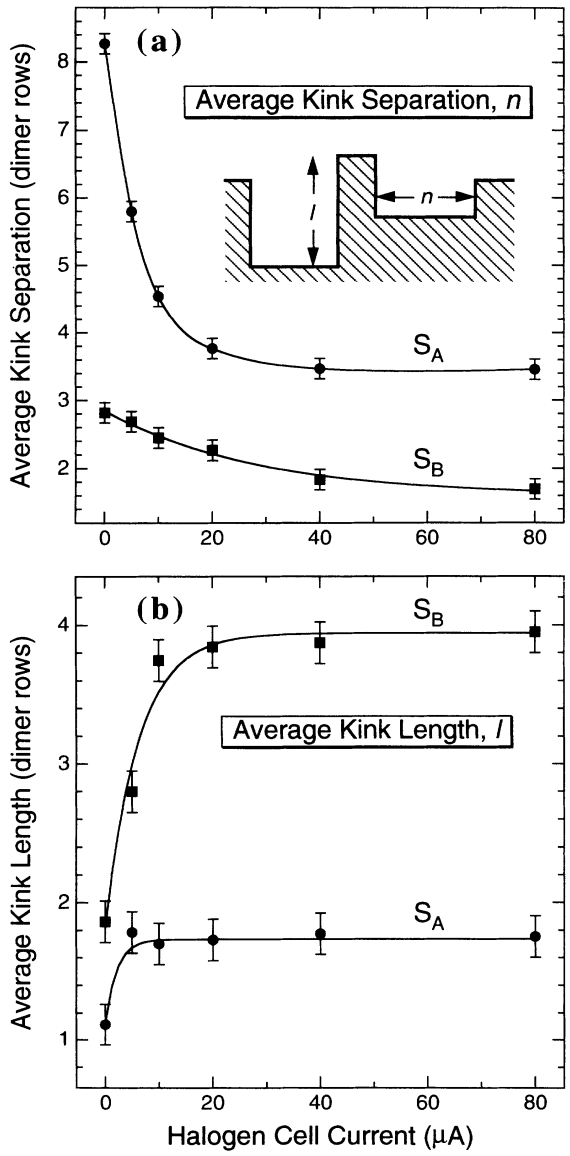

FIG. 6. (a) Average kink separations and (b) average kink lengths as functions of the Br_2 cell current for S_A and S_B step edges compared to those for clean Si(100), the zero of current. The inset in (a) defines kink separation n and kink length l in units of dimer rows. The results for average kink separation (a) demonstrate the systematic influence of flux on step profiles. Although the average kink length increases with Br_2 exposure (b), it depends only weakly on flux.

E. Discussion: terrace and step etching

The above experimental results and analysis of etch pits, surface defects, and step profiles make it possible to model the etching events as a function of temperature, fluence, and flux. We postulate that Br chemisorption to Si dangling bonds weakens dimer bonds and backbonds, making the surface susceptible to etching. We describe this spontaneous etching in terms of the statistical arrival, thermalization, and subsequent diffusion of bromine on the surface.

At low temperature and low fluence, one can envision the surface being subjected to an impinging Br_2 molecule that enters a molecular precursor state but then dissociates. In principle, the bonding site achieved after thermalization could correspond to a single Br atom on a Si dimer trapped on this dimer by a large barrier for diffusion. This appears not to be the case, however, since we find no evidence for isolated Br atoms bonded to Si dimers at the exposures investigated here. Instead, we find symmetric Si dimers with two adsorbed Br atoms. This suggests that Br atoms are sufficently mobile that the formation of more stable doubly occupied Si dimers is assured. Studies of Br-exposed Si at low temperature or very low fluence may reveal single Br species on a dimer.

With increasing Br_2 exposure at 300 K, the distance between doubly occupied dimers decreases, and the probability increases that an arriving Br_2 molecule will be within a diffusion length of the Br-terminated dimer. In this case, the spontaneous desorption of a volatile $SiBr_3$ or $SiBr_4$ molecule is possible. Energy released during formation of these species aids in the desorption through local heating and the weakening of Si-Si bonds, as shown in molecular dynamics calculations for atomic fluorine reactions on Si(100).[31] Such desorption will produce defects on the surface, and the defect density should increase with the fluence, as observed experimentally here.[11]

The role that native terrace defects play during molecular dissociation and the initial stages of etching is not easily characterized. Although Br-covered surfaces (Fig. 2) exhibit approximately three times as many defects as clean surfaces, many of the defects appear in groups as small vacancy islands. Hence many of the defects created upon adsorption may have been activated by existing defects. Although native surface defects may enhance volatile $SrBr_x$ formation, Si removal from a pristine terrace can still occur via the mechanism discussed above.

The effects of temperature are manifest in the images of Fig. 3 and those obtained at $T < 800$ K. In particular, we found minimal etching up to ~ 800 K, and images such as Fig. 3(a) showed that the surface consisted predominantly of stable dimers with a modest number of defects. Heating to 900 K changed the etched terrace morphology dramatically, as seen in Fig. 3(b). These effects can be rationalized in terms of the stability of the doubly occupied dimers, Br diffusion, and the strength of Si-Si bonds. At higher temperatures, the probability of Br detachment from a dimer will be greater, leading to enhanced diffusion and the chance of forming a volatile $SiBr_x$ species. Higher temperatures also weaken Si-Si bonds, making the surface more susceptible to etching.

Indeed, this manifests itself in TPD measurements that show that $SiBr_2$ becomes the dominant desorption product above ~ 800 K.[11] The removal of one of the dimer atoms frees the remaining Si atom, which is sufficiently mobile at 900 K that regrowth structures appear, as observed in Fig. 3(b). Ultimately, higher temperatures increase the yield of the etch products and Br_2 as well, resulting in Br depletion and a healing of the surface due to Si atom and vacancy diffusion and accommodation at step edges, as seen in Fig. 3(c).

This model can be extended to the etching of steps that are intrinsic to the clean surface and those that form the perimeters of single-layer etch pits. The results presented above demonstrate that the morphology of Si(100)-2×1 during the initial stages of etching is determined in part by the local instantaneous concentration of Br, a value that is dependent on the flux. The effect of flux on step-edge roughness is evident from the deviation-deviation correlation function (Fig. 5) and the average kink separation measurements (Fig. 6). In particular, the highly kinked S_B steps become rougher with increasing flux as etching into the terrace from random desorption sites at the edge occur. This roughness is less evident for the straighter S_A steps because Si removal is favored parallel to the dimer row direction along the step edge. In both cases, the roughness increases with flux.

The increase in step roughness reflects a complex interplay between three processes. The first involves the arrival rate of the incident Br_2 molecules. Locally higher concentrations of Br on terraces increase the probability of a random encounter between diffusing Br atoms and Br-terminated dimers, so that the formation of volatile, multiply halogenated silicon species is more likely. Were there no etching, the effect of the arrival rate would be small after exposure to equivalent fluences. In the presence of dynamic etching, however, the rate of arrival couples to the rate of material removal and the ability of the surface to heal etch damage at high temperature. The latter process involves atom diffusion and vacancy diffusion, both of which are anisotropic on Si(100)-2×1.[26,29] Although the fluence was fixed for our continuous etching experiments, the time spent at high temperature is inversely proportional to the flux. Thus, LF surfaces have more time to heal than do HF surfaces. We postulate that the observed behaviors of $G(r)$ and the average kink separation as a function of flux are related to the healing processes following volatile species formation. In particular, one can envision independent etch events at a step that create uncorrelated kinks when the local concentration is large. If these events occur on a time scale that is short compared to the ability of the step to eliminate the kink by Si diffusion or local rearrangement, then a rougher step profile will result. This rapid etching process then creates a configuration that is farther from equilibrium than that achieved at low etching rates, consistent with the observed morphological differences between LF and HF surfaces.

ACKNOWLEDGMENTS

This work was supported by the Office of Naval Research. We thank J. C. Patrin for contributions during the early stages of this work, and F. Stepniak for discussion.

[1]H. F. Winters and J. W. Coburn, Surf. Sci. Rep. **14**, 161 (1992), and references therein.
[2]J. J. Boland and J. S. Villarrubia, Phys. Rev. B **41**, 9865 (1990).
[3]J. C. Patrin, Y. Z. Li, M. Chander, and J. H. Weaver, Appl. Phys. Lett. **62**, 1277 (1993).
[4]J. C. Patrin and J. H. Weaver, Phys. Rev. B **48**, 17913 (1993).
[5]M. Chander, Y. Z. Li, J. C. Patrin, and J. H. Weaver, Phys. Rev. B **47**, 13035 (1993).
[6]M. Chander, Y. Z. Li, and J. H. Weaver, Phys. Rev. Lett. **71**, 4154 (1993).
[7]B. S. Swartzentruber, Y.-W. Mo, M. B. Webb, and M. G. Lagally, J. Vac. Sci. Technol. A **7**, 2901 (1989).
[8]N. D. Spencer, P. J. Goddard, P. W. Davies, M. Kitson, and R. M. Lambert, J. Vac. Sci. Technol. A **1**, 1554 (1983).
[9]M. Chander, Y. Z. Li, J. C. Patrin, and J. H. Weaver, Phys. Rev. B **48**, 2493 (1993).
[10]Z. Zhang and H. Metiu, Phys. Rev. B **48**, 8166 (1993).
[11]R. B. Jackman, R. J. Price, and J. S. Foord, Appl. Surf. Sci. **36**, 296 (1989).
[12]R. J. Hamers, P. Avouris, and F. Bozso, Phys. Rev. Lett. **59**, 2071 (1987).
[13]J. J. Boland, Phys. Rev. Lett. **67**, 1539 (1991).
[14]J. J. Boland, Phys. Rev. Lett. **65**, 3325 (1990).
[15]V. Eteläniemi, E. G. Michel, and G. Materlik, Surf. Sci. **251/252**, 483 (1991).
[16]J. A. Appelbaum, G. A. Baraff, and D. R. Hamann, Phys. Rev. B **14**, 588 (1976).
[17]U. Höfer, L. Li, and T. F. Heinz, Phys. Rev. B **45**, 9485 (1992).
[18]M. P. D'Evelyn, Y. L. Yang, and L. F. Sutcu, J. Chem. Phys. **96**, 852 (1991).
[19]R. J. Hamers, U. K. Köhler, and J. E. Demuth, Ultramicroscopy **31**, 10 (1989).
[20]J. Y. Tsao, E. Chason, U. Koehler, and R. Hamers, Phys. Rev. B **40**, 11951 (1989).
[21]Y.-W. Mo, B. Swartzentruber, R. Kariotis, M. B. Webb, and M. G. Lagally, Phys. Rev. Lett. **63**, 2393 (1989).
[22]Y.-W. Mo, R. Kariotis, B. S. Swartzentruber, M. B. Webb, and M. G. Lagally, J. Vac. Sci. Technol. A **8**, 201 (1990).
[23]J. J. Boland, Surf. Sci. **261**, 17 (1992).
[24]D. G. Cahill and P. Avouris, Appl. Phys. Lett. **60**, 326 (1992).
[25]N. Kitamura, M. G. Lagally, and M. B. Webb, Phys. Rev. Lett. **71**, 2082 (1993).

[26]P. Bedrossian and T. Klistner, Phys. Rev. Lett. **68**, 646 (1992).
[27]D. Rioux, R. J. Pechman, M. Chander, and J. H. Weaver (unpublished).
[28]C. Roland and G. H. Gilmer, Phys. Rev. B **46**, 13 437 (1992).
[29]Y.-W. Mo and M. G. Lagally, Surf. Sci. **248**, 313 (1991).
[30]H. J. W. Zandvliet, H. Wormeester, D. J. Wentink, and A. van Silfhout, Phys. Rev. Lett. **70**, 2122 (1993).
[31]P. C. Weakliem, C. J. Wu, and E. A. Carter, Phys. Rev. Lett. **69**, 200 (1992).

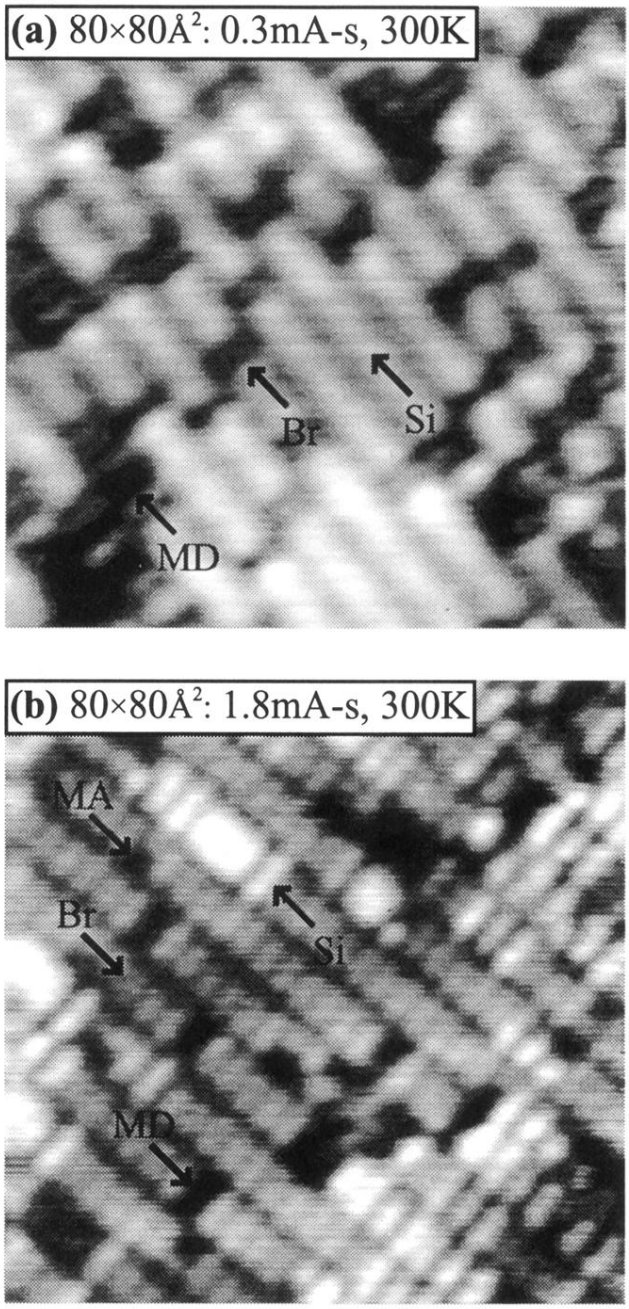

FIG. 1. Occupied-state images (−1.1 V, 0.2 nA) of Si(100)-2×1 exposed to Br_2 fluences of (a) 0.3 mA sec and (b) 1.8 mA sec at room temperature. The brightest features are clean Si dimers, labeled Si. Br adsorption sites (Br) are individually resolved and appear grey. Surface defects appear black, labeled MD for missing dimers and MA for missing atoms. Exposure to 1.8 mA sec produces a surface where the minority population corresponds to Si dimers that are Br free, as indicated by the bright features in (b).

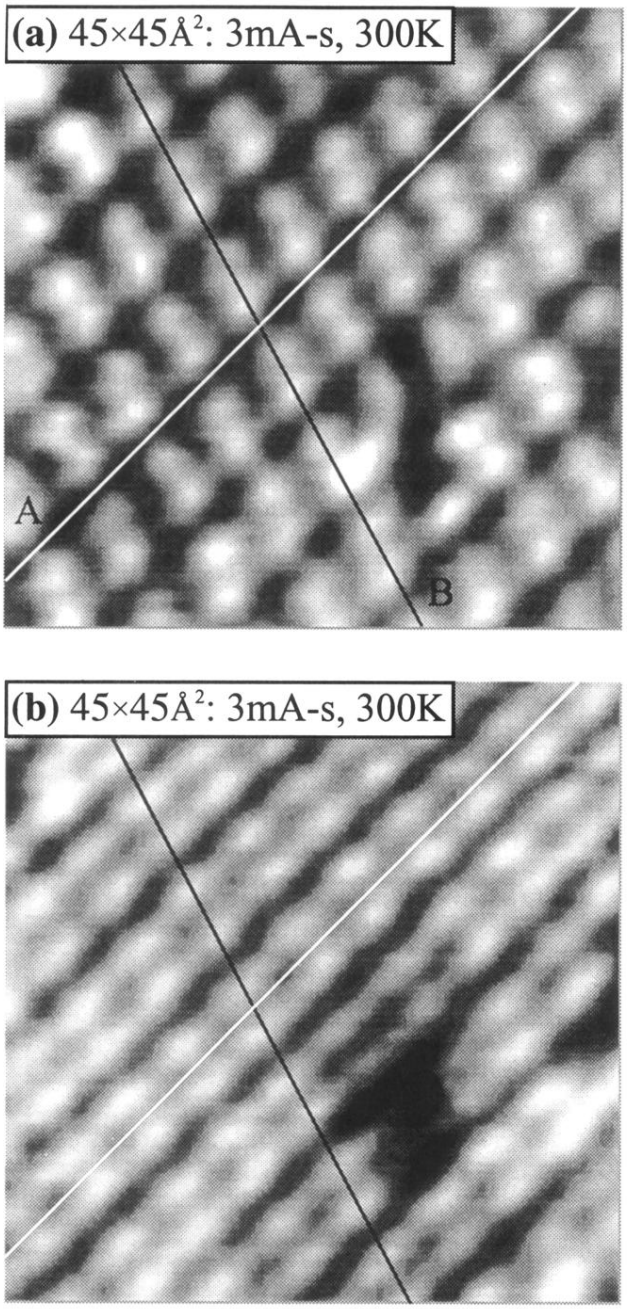

FIG. 2. Dual bias images (±0.9 V, 0.1 nA) of a Br-saturated Si(100)-2×1 surface after exposure to 3 mA sec. The bright features that appear in pairs are indicative of dissociative Br_2 chemisorption to dimer dangling bonds. Line *A* lies in the trough between dimers rows in both (a) and (b). Its position appears to be different, however, because the occupied and unoccupied states of the surface are not spatially coincident. Line *B* shows that the adsorption structure is parallel to the dimer-bond direction.

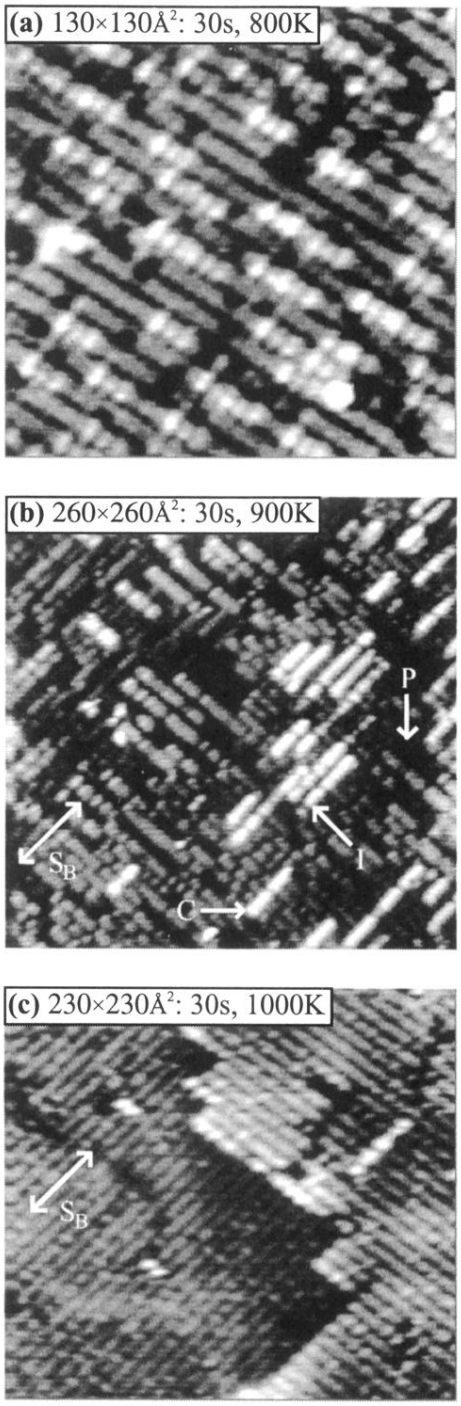

FIG. 3. Occupied-state images obtained after annealing a Br-covered surface for $800 \leq T \leq 1000$ K. (a) Bright features are clean Si dimers from which Br has been removed during processes that produce volatile etch products. (b) Terrace etching is apparent and the profile of the original S_B passing from lower left to upper right is poorly defined. Dimer chains (C) and 2×1 islands (I) have coalesced from material liberated during the etch. Single-layer etch pits (P) are apparent on the terraces. (c) The etch damage evident in (b) has largely been repaired by Si atom and vacancy diffusion, and most of the Br has desorbed.

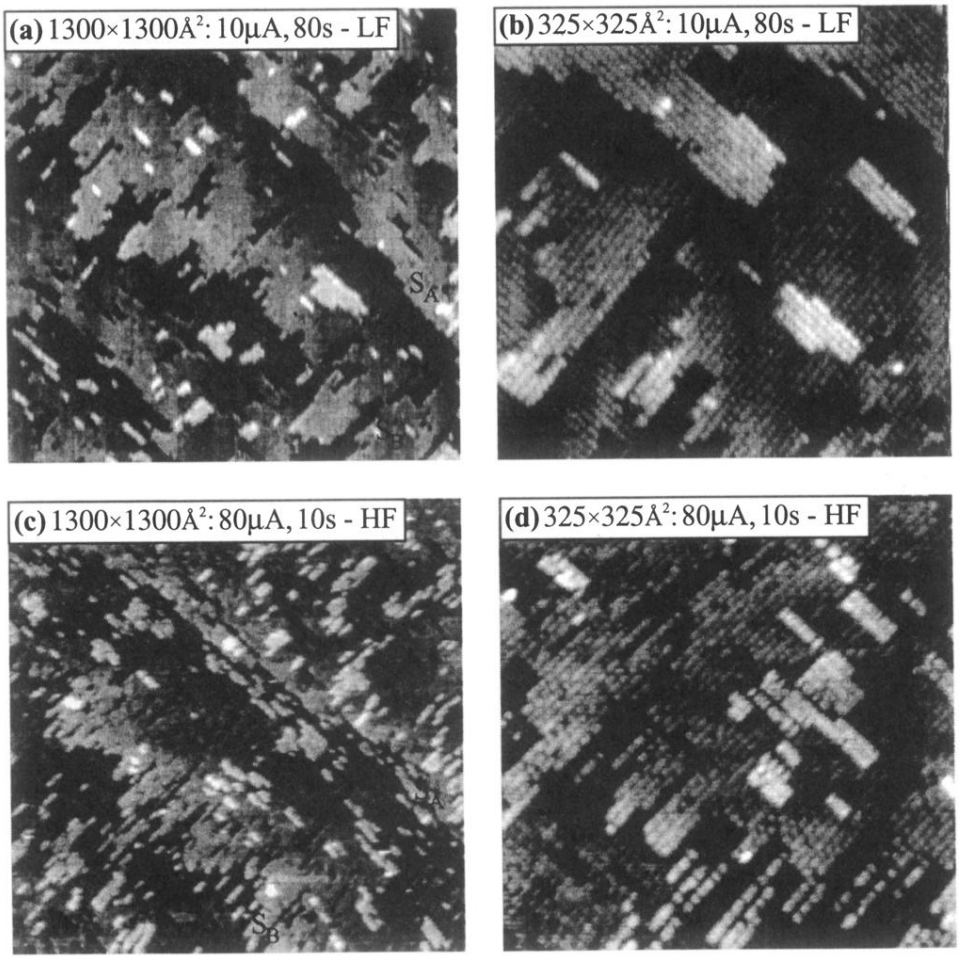

FIG. 4. Images taken after etching under conditions of LF [low flux, images (a) and (b)] and HF [high flux, images (c) and (d)] for times that produce the same fluence. The large-scale images show that the HF surfaces have rougher *B*-type step edges, a larger number of etch pits, and a greater amount of regrowth. The small-scale images show detailed differences in step-edge roughness and in regrowth structure morphology.